

## ARTICLES

**Crossed-Beam Reaction of Boron Atoms, B ( $^2P_j$ ), with Dimethylacetylene,  $CH_3CCCH_3$  ( $X^1A_{1g}$ ): Untangling the Reaction Dynamics to Form the 1,2-Dimethylene-3-bora-cyclopropane Molecule****D. Sillars and R. I. Kaiser\****Department of Chemistry, University of Hawaii, Honolulu, Hawaii 96822***N. Galland<sup>†</sup> and Y. Hannachi***Laboratoire de Physico-Chimie Moléculaire (CNRS UMR 5803) Université Bordeaux I, 351, Cours de la Libération, 330405 Talence Cedex, France**Received: November 21, 2002; In Final Form: March 31, 2003*

The reaction of ground-state boron atoms, B ( $^2P_j$ ), with dimethylacetylene,  $CH_3CCCH_3$  ( $X^1A_{1g}$ ), was studied at a collision energy of  $17.9 \text{ kJ mol}^{-1}$  using the crossed molecular beam approach. It was found that the reaction follows indirect scattering dynamics. B ( $^2P_j$ ) attacks the carbon–carbon triple bond of the dimethylacetylene molecule to form a cyclic  $BC_4H_6$  intermediate that undergoes hydrogen transfer from the methyl group to the boron atom. This complex then rotates around the *A/B* axis and fragments to atomic hydrogen plus a cyclic  $BC_4H_5$  isomer, 1,2-dimethylene-3-bora-cyclopropane, via a tight transition state.

**I. Introduction**

The reaction dynamics of ground-state boron atoms, B ( $^2P_j$ ), with hydrocarbon molecules are of inherent interest to the understanding of the chemical processes involved in the manufacture of semiconductors,<sup>1,2</sup> organoboron synthesis,<sup>3</sup> and boron combustion.<sup>4</sup> Electron-deficient bonding is a common feature in boron-rich solids, which would make it a logical choice for use in semiconductors.<sup>5</sup> One set of semiconductors that are currently of interest are the boron carbides.<sup>6</sup> They are very stable, possess high electrical as well as low thermal conductivities, and have been considered to be the most promising materials for realizing high-efficiency thermoelectric energy conversion given n-type boron carbides. These materials also have potential applications as high-temperature semiconductors.<sup>7</sup> Organoboron chemistry is another area that has received a great deal of interest from chemists over the last 50 years. Many efforts have been made to take advantage of the electron deficiency caused by the vacant p orbital on the boron atom of organoboranes and the metallic properties of boron derivatives.<sup>8</sup> A rich chemistry has developed around these properties, for instance, the hydroboration of alkenes and alkynes<sup>9</sup> or the allylation and propargylation of aldehydes with allylic and allenic boronic esters.<sup>10,11</sup> Following the spectacular development of radical chemistry in organic synthesis, the use of organoboranes has recently led to many novel and useful synthetic applications such as triethylborane as an initiator for radical chain reactions or a tin-free process for the formation of carbon–carbon bonds.<sup>12–14</sup> In particular, elemental boron is

appealing for use as an enhancing agent in combustion applications because of its high theoretical energy density both on a volumetric and a gravimetric basis.<sup>15</sup> This, coupled with a high energy of combustion process and low molecular weight products, explains why boron is considered to be an attractive material for use in rocket propellants and explosives.<sup>16,17</sup> Boron is also known to play an important biological role in many organisms, and recently the first example of an actual boron-containing biological molecule was discovered in the autoinducer AI-2 of the bacterium *Vibrio harveyi*.<sup>18</sup>

Because all of these macroscopic processes involving atomic boron are a complex series of bimolecular reactions, it is important to understand the underlying elementary steps involved. Therefore, an investigation of the basic mechanisms of these binary processes on a molecular level is crucial. The crossed molecular beam technique presents an unprecedented approach to the investigation of the chemical dynamics of bimolecular reactions.<sup>19</sup> Each reaction can be carried out under single-collision conditions. This means that there is neither collisional stabilization of potential intermediates nor successive reactions of the products with a third body. It also allows reactants to be formed in separate chambers under well-defined conditions such as velocity, velocity spread, and electronic states. Crossed-beam experiments further provide a method of identifying products with unknown spectroscopic properties by using a quadrupole mass spectrometer coupled to an electron impact ionizer.

The crossed-beam approach has been utilized previously to study the reactions of boron atoms, B ( $^2P_j$ ), with acetylene,  $C_2H_2$ - ( $X^1\Sigma_g^+$ )<sup>20</sup>, and ethylene,  $C_2H_4$  ( $X^1A_g$ )<sup>21</sup>, as simple representatives of alkynes and alkenes, respectively. The potential energy surface (PES) in Figure 1 shows the major reaction pathway

\* Corresponding author. E-mail: kaiser@gold.chem.hawaii.edu.

<sup>†</sup> Present address: Chemistry Department, King's College London, Strand WC2R 2LS, London, U.K.

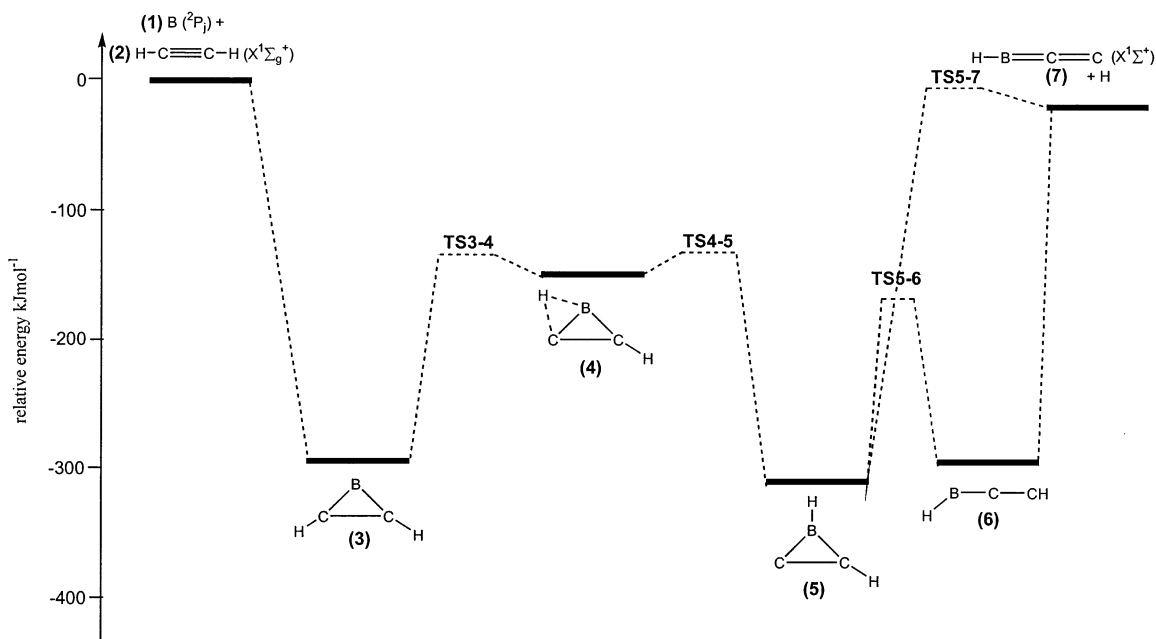


**Figure 1.** Schematic representation of the most important reaction pathway between  $B(^2P_j)$  and  $C_2H_2(X^1\Sigma_g^+)$  compiled from refs 20 and 22–24. TS denotes a transition state. Point groups are as follows: (2) =  $D_{\infty h}$ , (3) =  $C_{2v}$ , (4) =  $C_s$ , (5) =  $C_s$ , (6) =  $C_s$ , (7) =  $C_{\infty v}$ .

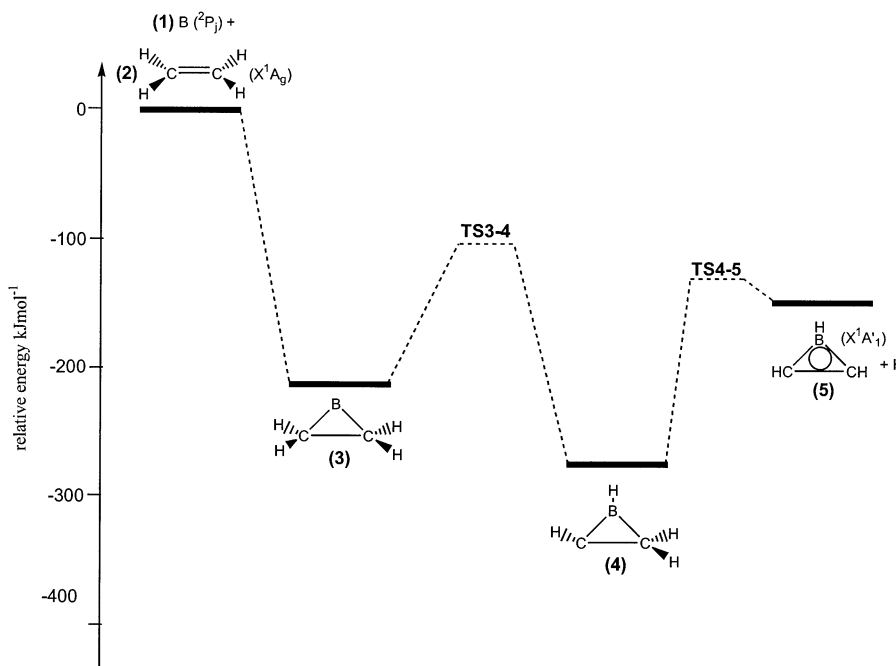


**Figure 2.** Schematic representation of the most important reaction pathway between  $B(^2P_j)$  and  $C_2H_4(X^1A_g)$  compiled from refs 21, 25, and 26. TS denotes a transition state. Point groups are as follows: (2) =  $D_{2h}$ , (3) =  $C_{2v}$ , (4) =  $C_1$ , (5) =  $C_{2v}$ .

that occurs between ground-state boron atoms,  $B(^2P_j)$  (1), and acetylene,  $C_2H_2(X^1\Sigma_g^+)$  (2). The mechanism involves the addition of the boron atom to the triple bond of acetylene without an entrance barrier to form a cyclic intermediate **3**. This is stabilized by  $297.1 \text{ kJ mol}^{-1}$  with respect to the reactants and then undergoes a hydrogen transfer via transition state **TS3-4**, which is  $158.9 \text{ kJ mol}^{-1}$  higher in energy than **3**. The process forms the bridged intermediate **4**; the latter rearranges through **TS4-5** located  $1.4 \text{ kJ mol}^{-1}$  above **4**. **TS5-6** connects to a linear  $BC_2H_2$  isomer **6** that is  $15.1 \text{ kJ mol}^{-1}$  less stable than **5**. A final hydrogen emission can proceed via **TS5-7** located  $6.6 \text{ kJ mol}^{-1}$  above the separated products or without a barrier, leading to the linear  $HBCC(X^1\Sigma^+)$  product. The overall reaction is

exothermic by  $6.9 \text{ kJ mol}^{-1}$  with respect to the reactants.<sup>20,22</sup> Note that species **3**, **5**, and **7** have been identified in an argon matrix and were characterized by infrared spectroscopy.<sup>23–25</sup>

Figure 2 depicts the pathway of the second reaction studied (i.e., between ground-state boron atoms,  $B(^2P_j)$  (1), and ethylene,  $C_2H_4(X^1A_g)$  (2)). The mechanism involves the addition of boron to the double bond of ethylene to form a cyclic intermediate **3**. The latter is stabilized by  $217.0 \text{ kJ mol}^{-1}$  with respect to the reactants and then undergoes a hydrogen shift via transition state **TS3-4**. This transition state is  $112.7 \text{ kJ mol}^{-1}$  higher in energy than **3** and connects to intermediate **4**. The final hydrogen loss leads to the cyclic, aromatic  $BC_2H_3(X^1A_1)$  (borirene) product through **TS4-5**. The overall reaction is exothermic by  $140.4 \text{ kJ}$

mol<sup>-1</sup> with respect to the reactants and has an exit barrier of 11.7 kJ mol<sup>-1</sup>.<sup>21,22</sup> The borirene molecule BC<sub>2</sub>H<sub>3</sub> (X<sup>1</sup>A<sub>1</sub>) was also the major reaction product observed in a low-temperature argon matrix.<sup>26,27</sup>

All reactions show common features. They have no entrance barrier, contain hydrogen migration(s), have bound reaction intermediates, and terminate with hydrogen losses. The reverse reactions (i.e., the addition of H to the closed-shell organoboron products) involve, with the exception of the H + HBCC → HBCC<sub>2</sub>H process as calculated at the B3LYP level, an entrance barrier. In this report, we investigate the bimolecular reaction of B (<sup>2</sup>P<sub>j</sub>) with dimethylacetylene, CH<sub>3</sub>CCCH<sub>3</sub> (X<sup>1</sup>A<sub>1g</sub>) to continue the research into important, elementary organoboron reactions. We will unravel the underlying reaction mechanism of the system and extract generalized principles for the reactions of boron with unsaturated hydrocarbons. Similarities and differences with the reactions of carbon with these unsaturated hydrocarbons can then be analyzed critically.

## II. Experimental Section

The reactive scattering experiments were performed in a universal crossed molecular beam apparatus described in ref 28. A pulsed supersonic boron, B (<sup>2</sup>P<sub>j</sub>), beam was generated via laser ablation of a boron rod at 266 nm.<sup>29</sup> The 30-Hz, 35–40 mJ output of a Spectra Physics GCR 270-30 Nd:YAG laser was focused onto a rotating boron rod, and ablated atoms were subsequently seeded into the helium gas released by a Proch-Trickl pulsed valve.<sup>30</sup> No boron clusters were present in the beam, and the intensities of the integrated time-of-flight (TOF)<sup>31</sup> spectra at mass-to-charge ratios (*m/e*) of 10 (<sup>10</sup>B<sup>+</sup>) and 11 (<sup>11</sup>B<sup>+</sup>) reflected the natural isotopic abundance ratio (80% <sup>11</sup>B vs 20% <sup>10</sup>B). The boron beam has a peak velocity (*v<sub>p</sub>*) of 1830 ± 40 ms<sup>-1</sup> and a speed ratio (*S*) of 7.8 ± 0.4. This beam crossed a pulsed dimethylacetylene beam (*v<sub>p</sub>* = 780 ± 10 ms<sup>-1</sup>, *S* = 8.4 ± 0.4) perpendicularly at an averaged collision energy of 17.9 ± 0.1 kJ mol<sup>-1</sup> in the interaction region of the crossed-beam machine. The scattered species were monitored by a triply differentially pumped ultrahigh vacuum (UHV) detector consisting of a Brink-type electron impact ionizer,<sup>32</sup> a quadrupole mass filter, and a Daly ion detector<sup>33</sup> operated in the TOF mode. Up to 330 000 TOF spectra were accumulated at each angle.

## III. Data Analysis

A forward-convolution routine<sup>34,35</sup> was used to fit the TOF spectra and the product angular distribution in the laboratory frame to reveal information on the velocity and angular distributions of the products in the center-of-mass coordinate system. This iterative method initially guesses the angular flux distribution *T*(θ) and the translational energy flux distribution *P*(*E<sub>T</sub>*) in the center-of-mass system (CM), which are assumed to be independent of each other. The symmetry of the scattering process around the relative velocity vector in the CM system restricts the angular dependence to θ because neither of the reactants is polarized. The *P*(*E<sub>T</sub>*) is chosen as a parametrized function:

$$P(E_T) = (E_T - B)^p X(E_{av} - E_T)^q \quad (1)$$

The *B* parameter is related to the exit barrier of the reaction with *B* = 0 for a simple bond rupture without an exit barrier. The first argument in eq 1 peaks at a finite value, *E<sub>p</sub>*, when *B* ≠ 0 and governs the energy difference between *E<sub>p</sub>* and the low-energy tail. The second argument describes a decaying function from *E<sub>p</sub>* to the end of the high-energy tail. *T*(θ) is de-

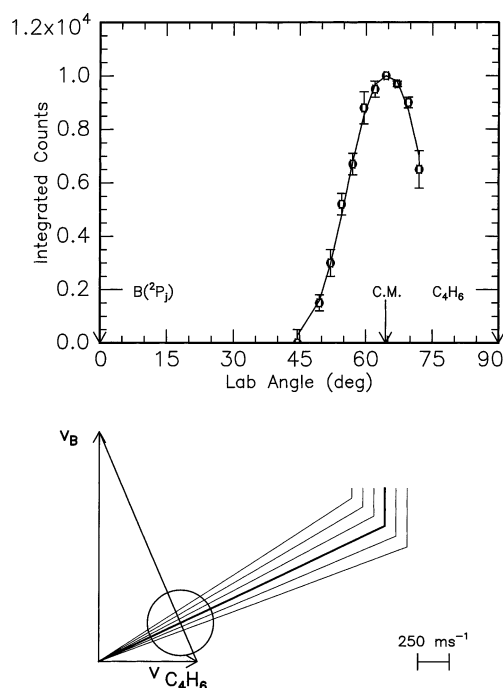


**Figure 3.** Lower: Newton diagram for the reaction B (<sup>2</sup>P<sub>j</sub>) + CH<sub>3</sub>CCCH<sub>3</sub> (X<sup>1</sup>A<sub>1g</sub>) at a collision energy of 17.9 kJ mol<sup>-1</sup>. The circle shows the maximum center-of-mass recoil velocity of the cyclic <sup>11</sup>BC<sub>4</sub>H<sub>5</sub> isomer assuming that no energy channels into the internal degrees of freedom. Upper: Laboratory angular distribution of the <sup>11</sup>BC<sub>4</sub>H<sub>5</sub> product at *m/e* = 63. Circles and 1σ error bars indicate experimental data, and the solid line indicates the calculated distribution. The center-of-mass angle is indicated by C.M. The solid lines originating in the Newton diagram point to distinct laboratory angles whose times of flight are shown in Figure 4.

defined as the sum of up to five Legendre polynomials *P<sub>i</sub>*(cos θ) with coefficients *a<sub>i</sub>*:

$$T(\theta) = \sum_{i=0}^4 a_i \times P_i(\cos \theta) \quad (2)$$

Laboratory TOF spectra and the laboratory angular distribution (LAB) were then calculated from the *T*(θ) and *P*(*E<sub>T</sub>*) distributions and were averaged over a grid of Newton diagrams. Each diagram defines the velocity and angular spread of each beam, the detector acceptance angle, and the ionizer length. Best fits were obtained by iteratively refining the Legendre coefficients and adjustable *P*(*E<sub>T</sub>*) parameters. We also generated product flux contour maps that showed the intensity of the reactively scattered products as a function of the center-of-mass scattering angle, θ, and product velocity, *u*, which is given by *I*(θ, *u*) ≈ *P*(*u*) *T*(θ).<sup>36</sup> This plot can be seen as an image of the reaction and contains all of the information on the scattering dynamics.

## IV. Results

**A. Reactive Scattering Signal.** Reactive scattering signals were observed at mass-to-charge (*m/e*) ratios of 64 (<sup>11</sup>BC<sub>4</sub>H<sub>5</sub><sup>+</sup>), 63 (<sup>11</sup>BC<sub>4</sub>H<sub>4</sub><sup>+</sup>/<sup>10</sup>BC<sub>4</sub>H<sub>5</sub><sup>+</sup>), 62 (<sup>11</sup>BC<sub>4</sub>H<sub>3</sub><sup>+</sup>/<sup>10</sup>BC<sub>4</sub>H<sub>4</sub><sup>+</sup>), 61 (<sup>11</sup>BC<sub>4</sub>H<sub>2</sub><sup>+</sup>/<sup>10</sup>BC<sub>4</sub>H<sub>3</sub><sup>+</sup>), and 60 (<sup>11</sup>BC<sub>4</sub>H<sup>+</sup>/<sup>10</sup>BC<sub>4</sub>H<sub>2</sub><sup>+</sup>). The relative intensities of these signals were measured as <0.05, 1.00, 0.88, 0.71, and 0.42, respectively. At each angle, the TOF spectra taken at different *m/e* ratios could be fit with the same center-of-mass functions, *T*(θ) and *P*(*E<sub>T</sub>*); therefore, the signal at lower *m/e* ratios must originate from the cracking of the <sup>11</sup>BC<sub>4</sub>H<sub>5</sub><sup>+</sup> parent ion in the ionizer. This suggests at the very least that the B vs H exchange channel is open. No radiative association to

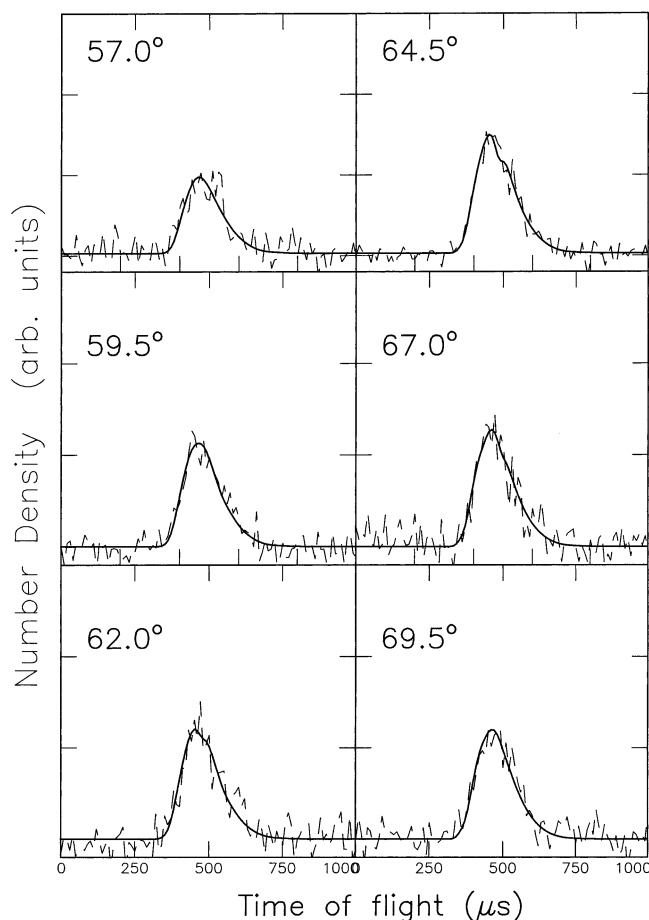


**Figure 4.** Time-of-flight data at  $m/e = 63$  for the indicated laboratory angles at a collision energy of  $17.9 \text{ kJ mol}^{-1}$ . The dashed line represents the experimental data, and the solid line represents the fit. Each TOF spectrum has been normalized to the relative intensity of each angle.

$\text{BC}_4\text{H}_6^+$  ( $m/e = 65$ ) or higher masses was detected. Consequently, data were taken at  $m/e = 63$  because of the highest signal-to-noise ratio at this mass-to-charge ratio.

**B. Laboratory Angular Distributions (LAB) and TOF Spectra.** Figure 3 shows the most probable Newton diagram for the title reaction and the laboratory angular (LAB) distribution of the  $^{11}\text{BC}_4\text{H}_5$  ( $m/e = 63$ ) product at a collision energy of  $17.9 \text{ kJ mol}^{-1}$ . TOF spectra are presented in Figure 4. The LAB distribution peaks at  $65^\circ$ , close to the center-of-mass angle of  $64.5 \pm 03^\circ$ , suggesting that the reaction proceeds through a complex via indirect reactive scattering dynamics. In addition, the narrow range of the LAB distribution of only  $27^\circ$  suggests that the averaged translational-energy release is relatively small.

**C. Center-of-Mass Translational Energy Distribution,  $P(E_T)$ .** The translational energy distribution,  $P(E_T)$ , is shown in Figure 5. The best fit of the LAB distribution and the TOF data could be achieved with a single  $P(E_T)$  that extends to a maximum translational energy release ( $E_{\text{max}}$ ) of  $114 \text{ kJ mol}^{-1}$ . The fit is relatively insensitive to the  $q$  parameter, and adding or cutting up to  $16 \text{ kJ mol}^{-1}$  in the long energy tail does not change the fit. Note that  $E_{\text{max}}$  is the sum of the reaction exoergicity and the collision energy. Therefore, by subtracting the collision energy from the high-energy cutoff, we are left with an experimental exoergicity of  $96 \pm 16 \text{ kJ mol}^{-1}$ . This experimental data can later be compared to ab initio calculations to identify the structural isomer(s). The fit was found to be very sensitive to the peak position. The  $P(E_T)$  peaks away from zero and shows a plateau between 17 and  $22 \text{ kJ mol}^{-1}$ , which suggests the presence of an exit barrier. Finally, the fraction of

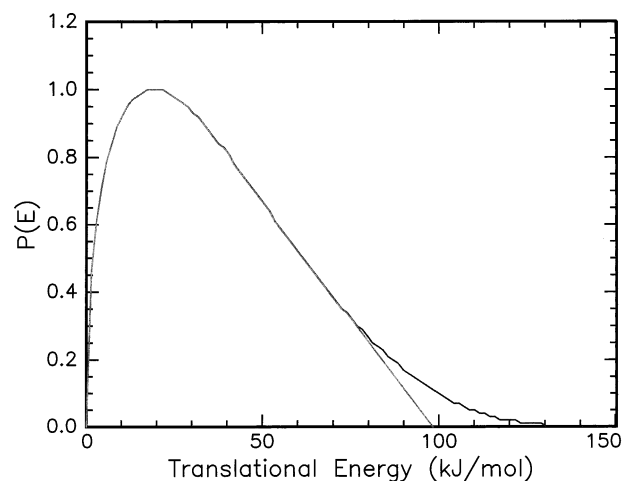


**Figure 5.** Center-of-mass translational energy flux distribution for the reaction  $\text{B} (^2\text{P}_j) + \text{CH}_3\text{CCCH}_3 (X^1\text{A}_{1g})$  at a collision energy of  $17.9 \text{ kJ mol}^{-1}$ . The two lines limit the range of acceptable fits to within  $1\sigma$  error bars.

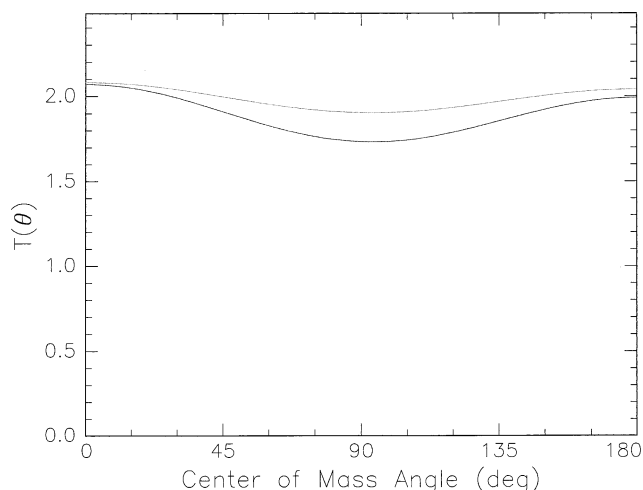


**Figure 6.** Center-of-mass angular flux distribution for the reaction  $\text{B} (^2\text{P}_j) + \text{CH}_3\text{CCCH}_3 (X^1\text{A}_{1g})$  at a collision energy of  $17.9 \text{ kJ mol}^{-1}$ . The two lines limit the range of acceptable fits to within  $1\sigma$  error bars.

energy channelled into the translational motion of the products was found to be  $33 \pm 3\%$ .

**D. Center-of-Mass Angular Distribution,  $T(\theta)$ , and Flux Contour Map,  $I(u, \theta)$ .** Figure 6 shows the center-of-mass angular distribution within the upper and lower error limits. Both distributions are almost symmetric around  $90^\circ$ . This feature implies that the lifetime of the decomposing complex(es) is longer than the rotational period. Figure 7 depicts two- and three-dimensional center-of-mass flux contour plots that demonstrate the forward-backward symmetric flux profile. The  $T(\theta)$ 's further show the maxima at both poles of  $0$  and  $180^\circ$  and depict minima at  $90^\circ$ . Ratios of flux intensities at  $0$  vs  $90^\circ$  and  $0$  vs  $180^\circ$  are  $0.85 \pm 0.07$  and  $1 \pm 0.02$ , respectively. The relatively moderate polarization of  $T(\theta)$  can be understood in terms of total angular momentum conservation. The total angular momentum  $\mathbf{J}$  is given by

$$\mathbf{J} = \mathbf{L} + \mathbf{j} = \mathbf{L}' + \mathbf{j}' \quad (3)$$

where  $\mathbf{L}$  and  $\mathbf{L}'$  are the initial and final orbital angular momenta and  $\mathbf{j}$  and  $\mathbf{j}'$  are the rotational angular momenta of the reactants and products, respectively. Equation 3 can be simplified by introducing the maximum impact parameter  $b_{\text{max}}$ , which can

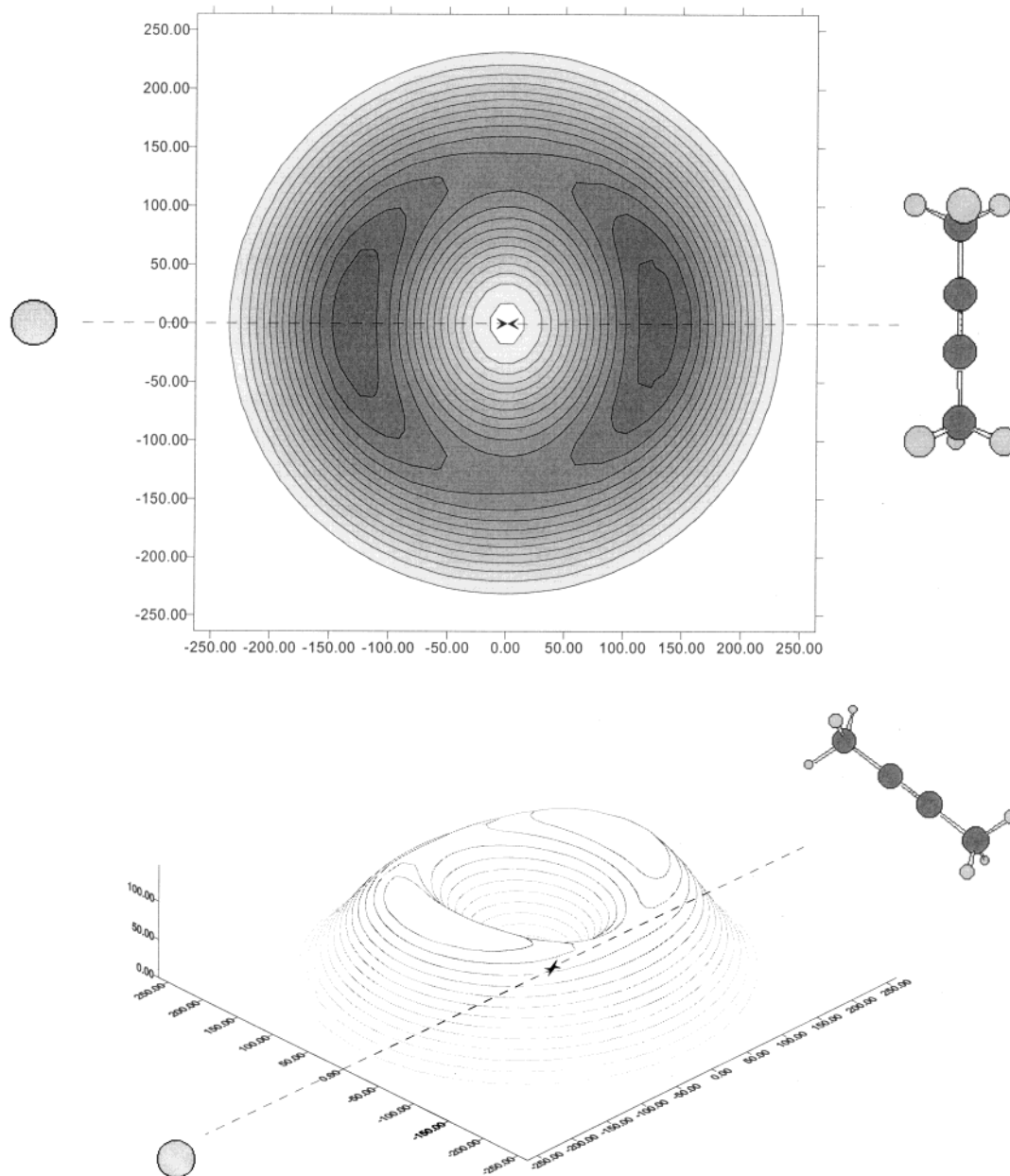


**Figure 7.** Best fit of the (top) two- and (bottom) three-dimensional flux contour maps for the reaction  $B(^2P_1) + CH_3CCCH_3(X^1A_{1g})$  at a collision energy of  $17.9 \text{ kJ mol}^{-1}$ . Units are  $\text{m s}^{-1}$ .

be derived for a barrierless entrance reaction of  $B + C_4H_6$  from ref 37. Utilizing the ionization potentials of atomic boron and dimethylacetylene,  $E_{B(^2P_1)} = 8.3 \text{ eV}$  and  $E_{C_4H_6} = 9.6 \text{ eV}$ , and their polarizabilities,  $\alpha_{B(^2P_1)} = 3 \times 10^{-30} \text{ m}^3$  and  $\alpha_{C_4H_6} = 8.2 \times 10^{-30} \text{ m}^3$ ,<sup>38</sup>  $b_{\text{max}}$  must be equal to  $3 \text{ \AA}$ . The maximum orbital angular momentum  $L_{\text{max}}$  relates to  $b_{\text{max}}$ :

$$\mathbf{L}_{\text{max}} = \mu b_{\text{max}} \mathbf{v}_r \quad (4)$$

Here,  $\mu$  is the reduced mass, and  $v_r$ , the relative velocity of the reactants. Accounting for these data gives us  $L_{\text{max}} \approx 85\hbar$ .  $C_4H_6$  is produced in a supersonic expansion limiting the rotational energy to  $3\hbar$ , which makes it possible to simplify eq 3 to

$$\mathbf{L} \approx \mathbf{J} = \mathbf{L}' + \mathbf{j}' \quad (5)$$

Now we estimate the final orbital angular momentum  $L'$ . Here the relative velocity of the products corresponds to the average

translational energy release, which is calculated in section IV.C from the PES. The exit barrier  $b'_{\text{max}}$  is taken as  $2.5 \text{ \AA}$  (i.e., the impact parameter for the reverse reaction of an H atom with the  $BC_4H_5$  product isomer). This gives  $L' \approx 33\hbar$ . Because  $L' \approx 0.4L$ , the reaction is governed by a moderate  $L$  and  $L'$  coupling and hence a visible polarization of  $T(\theta)$ . This leaves  $52\hbar$  to go into the rotational angular momentum of the product. The peaks at  $0$  and  $180^\circ$  in  $T(\theta)$  suggest that the H atom leaves the decomposing complex perpendicular to the total angular momentum (i.e., in the plane of the rotating intermediate).

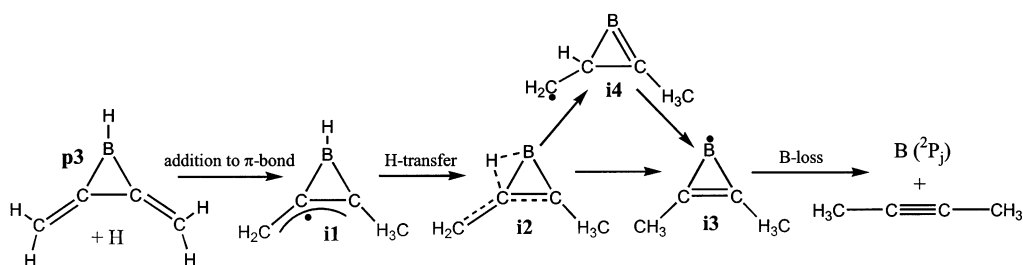
## V. Discussion

**A. Identification of Reaction Product(s).** The first step in finding the actual reaction mechanism is to expose the reaction product. For this, we contrast the experimentally determined reaction energy with those for different isomers determined from ab initio calculations. Here, stationary points on the  $BC_4H_5$  surface have first been located at the B3LYP/cc-pVDZ level of

**TABLE 1:** Calculated Reaction Energies to Form Three Possible  $C_4H_5B$  Isomers Plus Atomic Hydrogen Using G2, G3, and CCSD(T)/cc-pVTZ//B3LYP/cc-pVDZ Levels of Theory<sup>a</sup>

	<b>p1</b>	<b>p2</b>	<b>p3</b>
G2 (kJ mol <sup>-1</sup> )	-151.3	-138.3	-80.4
G3 (kJ mol <sup>-1</sup> )	-157.5	-145.0	-83.4
CCSD(T)/cc-pVTZ//B3LYP/ cc-pVDZ (kJ mol <sup>-1</sup> )	-141.6	-127.8	-69.6

<sup>a</sup> Zero-point vibration energy corrections of the reactants and products are included.

**Figure 8.** Suggested mechanism for the reverse reaction between the cyclic  $BC_4H_5$  structure (**p3**) and a hydrogen atom.

theory.<sup>39,40</sup> The harmonic frequencies were calculated at the same level to characterize the stationary points (minima versus transition state) to obtain zero-point vibrational energy (ZPVE). Total energies were refined at the CCSD(T)/cc-pVTZ level<sup>41</sup> using B3LYP/cc-pVDZ optimized geometries with B3LYP/cc-pVDZ ZPVE corrections. The reaction energies have also been computed using composite G2 (ref 42a) and G3 (ref 42b) methods, which are known to be an accurate and efficient procedure for the prediction of molecular thermochemistry. All calculations were conducted with Gaussian 98.<sup>43</sup> The calculated reaction energies are reported in Table 1. The obtained G2 and G3 values are larger than the corresponding CCSD(T)/cc-pVTZ//B3LYP/cc-pVDZ values.

The translational-energy distribution shows that the formation of the  $BC_4H_5$  isomer(s) is exoergic by  $96 \pm 16$  kJ mol<sup>-1</sup> (sections IV.B and IV.C). The electronic structure calculations found three low-lying  $BC_4H_5$  isomers, **p1**–**p3**. The **p1** structure is the most stable isomer, and the reaction exoergicities to form **p1** + H is calculated to lie between 141.6 and 157.5 kJ mol<sup>-1</sup>. The **p2** isomer is less stable than **p1** by about 13 kJ mol<sup>-1</sup>. The cyclic structure **p3** is the least stable isomer; reaction exoergicities to synthesize **p3** + H were derived to be between 69.6 and 83.4 kJ mol<sup>-1</sup>. By comparing the experimental data with the ab initio values in Table 1, it is obvious that **p3** is the most likely reaction product. As in the case of the B + C<sub>2</sub>H<sub>2</sub> reaction product, the GX-obtained ( $X = 2, 3$ ) exoergicities is in much better agreement with the experimentally derived value than the one obtained at the single-point CCSD(T)/cc-pVTZ//B3LYP/cc-pVDZ level.

Also, the  $P(E_T)$  peaks away from zero translational energy at 17–22 kJ mol<sup>-1</sup>, which suggests the presence of an exit barrier if the intermediate decomposes to **p3** + H. Because **p3** is an unsaturated closed-shell product, the principle of microscopic reversibility of an addition of the hydrogen atom to an unsaturated bond of the cyclic structure dictates that this reverse process should have an entrance barrier. We can compare this order of magnitude with barriers of related reactions (i.e., the H-atom addition to acetylene (3–13 kJ mol<sup>-1</sup>), ethylene (4–19 kJ mol<sup>-1</sup>), and benzene (14–22 kJ mol<sup>-1</sup>) to show that the experimental value is a reasonable one.<sup>44</sup>

**B. Mechanistic Information.** The shape of  $T(\theta)$  (section IV.D) demonstrates that a  $BC_4H_6$  intermediate is formed. This complex has a lifetime within the order of its rotational period, which means that the reaction dynamics must be classified as indirect. On the basis of this information, we now attempt to unravel the underlying mechanism for the formation of **p3**. For this, we first compare the structure of the dimethylacetylene reactant with that of the **p3** reaction product. The **p3** isomer carries no methyl group; to connect **p3** to the dimethylacetylene reactant via distinct intermediates, it is likely that in the reverse reaction a hydrogen atom adds to the carbon–carbon double bond at the exocyclic CH<sub>2</sub> moiety. This could form intermediate **i1** via an entrance barrier (Figure 8). The next step links **i1** with dimethylacetylene. This process likely involves a hydrogen migration from the boron atom to the remaining exocyclic CH<sub>2</sub> group to give an intermediate **i3**. It could occur either in a single step via a bicyclic intermediate **i2** (which is similar to the one formed in the reaction between B and C<sub>2</sub>H<sub>2</sub>, section I) or by a two-step mechanism via intermediates **i2** and **i4**. The final step would be the release of atomic boron from **i3** to produce the reactants. On the basis of these considerations, the following reaction dynamics are likely. The boron atom adds to the  $\pi$  bond of dimethylacetylene to form intermediate **i3**. The latter then undergoes hydrogen migration(s) possibly via a bicyclic intermediate **i2** to form **i1**. This cyclic intermediate then loses a hydrogen atom from the methyl group via an exit barrier of between 17 and 22 kJ mol<sup>-1</sup> to form **p3**.

The remaining question to be solved is why the peaks in  $T(\theta)$  are found at both poles of 0 and 180°. This finding suggests that the hydrogen atom leaves intermediate **i1** perpendicular to the total angular momentum vector **J**. We investigate first whether **p3** could rotate around its *C* axis, which is parallel to **J**. This would require that in the reversed reaction the hydrogen atom approaches almost parallel to **J** because some electron density of the  $\pi$  orbital of the unsaturated bonds is also parallel to the *C* axis. This means that in the forward reaction the hydrogen atom would be emitted parallel to the total orbital angular momentum vector **J**, and  $T(\theta)$  would peak at 90°. <sup>45</sup> This is clearly not observed experimentally; therefore, we conclude that the contribution of **p3** excited to *C* rotation is only minor.

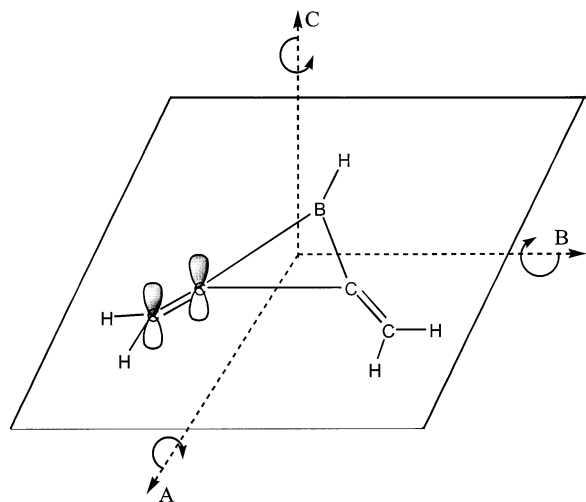


**Figure 9.** Schematic representation of the location of the three principal axes and the rotations of the complex around A, B, and C.

Assuming that **J** is almost parallel to either the A or B axis of **p3**, the H atom can add perpendicular to **J** to form **i1**. For the forward reaction, this would result in the emission of the H atom from **i1** with maxima at center-of-mass angles of 0 and 180° as found experimentally. We therefore expect most of the **p3** products to be excited to A- and/or B-like rotations. Furthermore, we analyze distinct rotational axes of the products.

**C. Alternative C<sub>4</sub>H<sub>5</sub>B Product Isomers, p1 and p2.** We now look at why isomers **p1** and **p2** are, if any, only minor reaction products using a similar approach to that in section V.C. Dimethylacetylene can be connected to the **p1** and **p2** products first by an addition of the boron atom to the  $\pi$  bond to form **i3**. In both the **p1** and **p2** structures, the methyl group is conserved and adjacent to the boron atom. This suggests that a methyl group migration must be involved to produce **i6**. Again, this step could proceed via the formation of bicyclic intermediate **i5**. **i6** could ring open to form intermediate **i7**. Hydrogen loss from the methyl group attached to the carbon atom would then create isomer **p2**, whereas H loss from the methyl group at the boron atom would form **p1**. However, the limiting factor of the proposed mechanisms to synthesize **p1** and **p2** is the

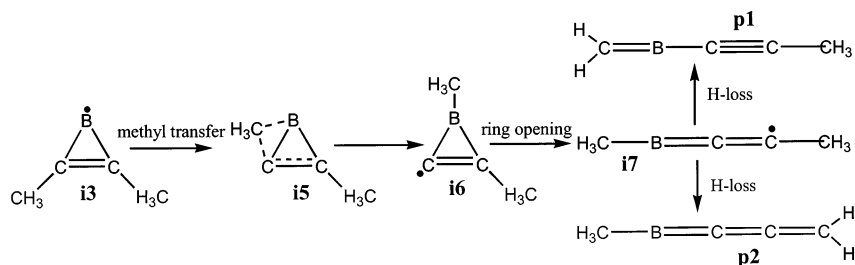


**Figure 10.** Proposed reaction for the formation of isomers **p1** and **p2**.

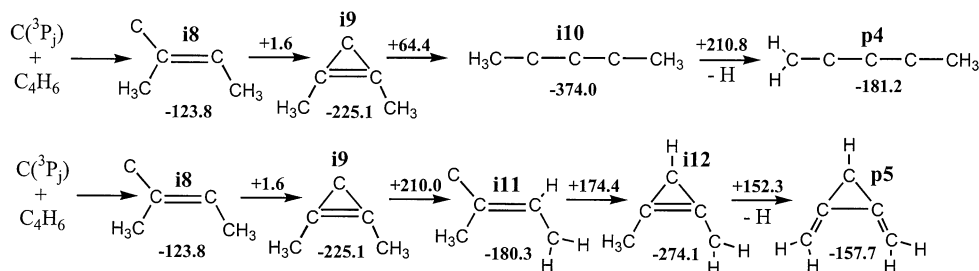


**Figure 11.** Schematic representation of the two mechanisms in the reaction between atomic carbon and dimethylacetylene to form different C<sub>5</sub>H<sub>5</sub> isomers. The values above the arrows show the barrier heights with respect to the previous intermediate, and those below each structure show its energy of formation with respect to the reactants. All values are given in kJ mol<sup>-1</sup>.

migration of the bulky methyl group. This would have an intrinsically larger barrier compared to that of the facile H migration involved in the formation of **p3**; therefore, the pathways to **p1** and **p2** are likely to be closed.

**D. Comparison with the Reaction of C(<sup>3</sup>P<sub>j</sub>) with Dimethylacetylene.** The equivalent reaction between a carbon atom and dimethylacetylene has been studied previously under similar conditions and showed similarities and differences to our experimental results.<sup>46</sup> Figure 11 shows the two pathways for the reaction between C(<sup>3</sup>P<sub>j</sub>) and dimethylacetylene. This mechanism also starts with the addition of a carbon atom to the  $\pi$  bond of dimethylacetylene in a manner similar to that observed for boron in the title reaction. Note, however, that **i9** can also be formed without **i8**. The preferred reaction of **i9** is a ring opening to **i10**, followed by the loss of hydrogen to produce the product, **p4**. This pathway has been observed to be the major route under single-collision conditions. The second pathway is comparable to the equivalent reaction with boron in that after the addition to the  $\pi$  bond it proceeds via hydrogen migration to **i11** or **i12** and hydrogen loss to form a cyclic product, **p5**. The barrier for hydrogen migration from **i9** to **i12** is larger by 110 kJ mol<sup>-1</sup> than that for the ring-opening step from **i9** to **i10**. This is dramatically different from the boron and dimethylacetylene reaction where the barrier to hydrogen transfer is suspected to be lower than that for ring opening.

## VI. Conclusions

The reaction of ground-state boron atoms, B(<sup>2</sup>P<sub>j</sub>), with dimethylacetylene, CH<sub>3</sub>CCCH<sub>3</sub> (X<sup>1</sup>A<sub>1g</sub>), was studied at a collision energy of 17.9 kJ mol<sup>-1</sup> using the crossed molecular beam technique. It was found that the reaction follows indirect scattering reaction dynamics. The obtained data suggest that the reaction is barrierless, as in the case of the B + C<sub>2</sub>H<sub>2</sub> and B + C<sub>2</sub>H<sub>4</sub> reactions.<sup>20–22</sup> This process forms a cyclic intermediate through the addition of boron to the carbon–carbon triple bond. Hydrogen transfer from a methyl group to the boron atom forms a second intermediate, which then fragments to atomic hydrogen and BC<sub>4</sub>H<sub>5</sub> via an exit barrier of between 17 and 22 kJ mol<sup>-1</sup> with respect to the products. It was found that before fragmentation this intermediate initially rotates in a plane roughly parallel to **J** around its A or B axis.

The reactions of ground-state boron and carbon with ethylene, acetylene, and dimethylacetylene have now all been studied.<sup>47,48</sup> On the basis of this research, we can say that, in general, the reaction of boron or carbon with an unsaturated hydrocarbon proceeds via addition to the multiple bond. The reaction with boron then forms a cyclic intermediate that undergoes hydrogen transfer and then hydrogen loss to give a cyclic product (ethylene and dimethylacetylene reactions) and a linear HBCC molecule in the case of the acetylene reactant. However, the reaction with carbon, with the exception of the C/C<sub>2</sub>H<sub>2</sub> system, continues with a ring-opening step followed by hydrogen loss to give products. Further research in this area, such as investigating the reactions between boron and allene or boron and methylacetylene, should be performed in order to confirm this general mechanism.

**Acknowledgment.** Y.H. thanks IDRIS (CNRS), project 337, for computer facilities. This work was further supported by The University of Hawaii.

## References and Notes

- (1) Taniguchi, T.; Tanaka, J.; Mishima, O.; Ohsawa, T.; and others. *Appl. Phys. Lett.* **1993**, *62*, 576.
- (2) Sugino, T.; Tai, T.; Etou, Y. *Diamond and Related Materials* **2001**, *10*, 1375.
- (3) Zhdankin, V. V.; Persichini, P. J.; Zhang, L.; Fix, S.; and others. *Tetrahedron Lett.* **1999**, *40*, 6705.
- (4) Foelsche, R. O.; Burton, R. L.; Krier, H. *Combust. Flame* **1999**, *117*, 32.
- (5) Aoyama, T.; et al. *J. Electrochem. Soc.* **1998**, *145*, 689.
- (6) Albert, B.; Schmitt, K. *Inorg. Chem.* **1999**, *38*, 6159.
- (7) Liu, C. H. *Mater. Lett.* **2001**, *49*, 308.
- (8) Albrecht, K.; et al. *J. Chem. Soc., Perkin Trans. 2* **2000**, *10*, 2153.
- (9) Brown, H. C.; Blue, C. D.; Nelson, D. J.; Bhat, N. G. *J. Org. Chem.* **1989**, *54*, 6064.
- (10) Brown, H. C.; Vasumathi, N.; Joshi, N. N. *Organometallics* **1993**, *12*, 1058.
- (11) Ueda, M.; Saitoh, A.; Miyaura, N. *J. Organomet. Chem.* **2002**, *642*, 145.
- (12) Ollivier, C.; Renaud, P. *Chem. Rev.* **2001**, *101*, 3415.
- (13) Pokidova, T. S.; Denisov, E. T. *Russ. Chem. Bull.* **2001**, *50*, 390.
- (14) Cadot, C.; Cossy, J.; Dalko, P. I. *Chem. Commun.* **2000**, *12*, 1017.
- (15) Politzer, P.; Lane, P.; Concha, M. C. *J. Phys. Chem. A* **1999**, *103*, 1419.
- (16) Ulas, A.; Kuo, K. K.; Gotzmer, C. *Combust. Flame* **2001**, *127*, 1935.
- (17) Dreizin, E. L.; Keil, D. G.; Felder, W.; Vicenzi, E. P. *Combust. Flame* **1999**, *119*, 272.
- (18) Chen, X.; Schauder, S.; Potier, N.; Dorsselaer, A. V.; Pelezer, I.; Bassler, B. L.; Hughson, F. M. *Nature* **2002**, *415*, 545.
- (19) Scoles, G. *Atomic and Molecular Beam Methods*; Oxford University Press: New York, 1988.
- (20) Balucani, N.; Osvany, O.; Lee, Y. T.; Kaiser, R. I.; Galland, N.; Rayez, M. T.; Hannachi, Y. *J. Comput. Chem.* **2001**, *22*, 1359. Kaiser, R. I.; Balucani, N.; Galland, N.; Caralp, F.; Rayez, M. T.; Hannachi, Y. *J. Phys. Chem.* Submitted.
- (21) Balucani, N.; Asvany, O.; Lee, Y. T.; Kaiser, R. I.; Galland, N.; Hannachi, Y. *J. Am. Chem. Soc.* **2000**, *122*, 11234.
- (22) Galland, N. Ph.D. Thesis, Université Bordeaux 1, Cedex, France, 2002.
- (23) Andrews, L.; Hassanzadeh, P.; Martin, J. M. L.; Taylor, P. R. *J. Phys. Chem.* **1993**, *97*, 5839.
- (24) Flores, J. R.; Largo, A. *J. Phys. Chem.* **1992**, *96*, 3015.
- (25) Martin, J. M. L.; Taylor, P. R.; Hassanzadeh, P.; Andrews, L. *J. Am. Chem. Soc.* **1993**, *115*, 2511.
- (26) Galland, N.; Hannachi, Y.; Lanzisera, D. V.; Andrews, L. *Chem. Phys.* **1998**, *230*, 143.
- (27) Andrews, L.; Lanzisera, D.; Hassanzadeh, P.; Hannachi, Y. *J. Phys. Chem. A* **1998**, *102*, 3259.
- (28) Lee, Y. T.; McDonald, J. D.; LeBreton, P. R.; Herschbach, D. R. *Rev. Sci. Instrum.* **1969**, *40*, 1402.
- (29) Kaiser, R. I.; Suits, A. G. *Rev. Sci. Instrum.* **1995**, *66*, 5405.
- (30) Proch, D.; Trickl, T. *Rev. Sci. Instrum.* **1989**, *60*, 713.
- (31) Parson, J. M.; Shobatake, K.; Lee, Y. T.; Rice, S. A. *J. Chem. Phys.* **1973**, *59*, 1402.
- (32) Brink, G. O. *Rev. Sci. Instrum.* **1966**, *37*, 857.
- (33) Daly, N. R. *Rev. Sci. Instrum.* **1960**, *31*, 264.
- (34) Weis, M. S. Ph.D. Thesis, University of California, Berkeley, CA, 1986.
- (35) Vernon, M. Thesis, University of California, Berkeley, CA, 1981.
- (36) Kaiser, R. I. *Acc. Chem. Res.* **2001**, *34*, 699.
- (37) Levine, R. D.; Bernstein, R. B. *Molecular Reaction Dynamics and Chemical Reactivity*; Oxford University Press: Oxford, U.K., 1987.
- (38) Keir, R. I.; Lamb, D. W.; Ritchie, G. L. D.; Watson, J. N. *Chem. Phys. Lett.* **1997**, *279*, 22.
- (39) Becke, A. D. *J. Chem. Phys.* **1993**, *98*, 5648. Lee, C.; Yang, W.; Parr, R. G. *Phys. Rev. B* **1988**, *37*, 785. Stevens, P. J.; Devlin, F. J.; Chabalowski, F.; Frisch, M. J. *J. Phys. Chem.* **1994**, *98*, 11623.
- (40) Dunning, T. H. *J. Chem. Phys.* **1998**, *90*, 1007.
- (41) Raghavachari, K.; Trucks, G. W.; Pople, J. A.; Head-Gordon, M. *Chem. Phys. Lett.* **1989**, *157*, 479.
- (42) Curtiss, L. A.; Raghavachari, K.; Redfern, P. C.; Rassolov, V.; Pople, J. A. *J. Chem. Phys.* **1991**, *94*, 7221. (b) Curtiss, L. A.; Raghavachari, K. In *Quantum Mechanical Electronic Structure: Calculations with Chemical Accuracy*; Langhoff, S. R., Ed.; Kluwer Academic Publishers: Dordrecht, The Netherlands, 1995. (c) Raghavachari, K.; Curtiss, L. A. In *Modern Electronic Structure Theory*; Yarkony, D. R., Ed.; World Scientific: Singapore, 1995.
- (43) Frisch, M. J.; Trucks, G. W.; Schlegel, H. B.; Scuseria, G. E.; Robb, M. A.; Cheeseman, J. R.; Zakrzewski, V. G.; Montgomery, J. A., Jr.; Stratmann, R. E.; Burant, J. C.; Dapprich, S.; Millam, J. M.; Daniels, A. D.; Kudin, K. N.; Strain, M. C.; Farkas, O.; Tomasi, J.; Barone, V.; Cossi, M.; Cammi, R.; Mennucci, B.; Pomelli, C.; Adamo, C.; Clifford, S.; Ochterski, J.; Petersson, G. A.; Ayala, P. Y.; Cui, Q.; Morokuma, K.; Malick, D. K.; Rabuck, A. D.; Raghavachari, K.; Foresman, J. B.; Cioslowski, J.; Ortiz, J. V.; Stefanov, B. B.; Liu, G.; Liashenko, A.; Piskorz, P.; Komaromi, I.; Gomperts, R.; Martin, R. L.; Fox, D. J.; Keith, T.; Al-Laham, M. A.; Peng, C. Y.; Nanayakkara, A.; Gonzalez, C.; Challacombe, M.; Gill, P. M. W.; Johnson, B. G.; Chen, W.; Wong, M. W.; Andres, J. L.; Head-Gordon, M.; Replogle, E. S.; Pople, J. A. *Gaussian 98*, revision A.7; Gaussian, Inc.: Pittsburgh, PA, 1998.
- (44) Mallard, W. G.; Westley, F.; Herron, J. T.; Hampson, R. F. *NIST Chemical Kinetics Database*, version 6.0; National Institute of Standards and Technology: Gaithersburg, MD, 1994.
- (45) Levine, R. D.; Bernstein, R. B. *Molecular Reaction Dynamics and Chemical Reactivity*; Oxford University Press: New York, 1987.
- (46) Huang, L. C. L.; Lee, H. Y.; Mebel, A. M.; Lin, S. H.; Lee, Y. T.; Kaiser, R. I. *J. Chem. Phys.* **2000**, *113*, 9637.
- (47) Kaiser, R. I.; Lee, Y. T.; Suits, A. G. *J. Chem. Phys.* **1996**, *105*, 8705.
- (48) Kaiser, R. I.; Ochsenfeld, C.; Head-Gordon, M.; Lee, Y. T.; Suits, A. G. *J. Chem. Phys.* **1997**, *106*, 1729.